International Journal of Naval Architecture and Ocean Engineering 12 (2020) 343–353

Contents lists available at ScienceDirect

International Journal of Naval Architecture and Ocean Engineering

journal homepage: http://www.journals.elsevier.com/international-journal-of-naval-architecture-and-ocean-engineering/

Vibro-acoustic modelling of immersed cylindrical shells with variable thickness

Xianzhong Wang [a, b, *], Hongzhou Lin [c], Yue Zhu [c], Weiguo Wu [a, c]

[a] Key Laboratory of High Performance Ship Technology (Wuhan University of Technology), Ministry of Education, Wuhan 430063, China
[b] Faculty of Engineering and Physical Sciences, University of Southampton, Southampton SO16 7QF, UK
[c] School of Transportation, Wuhan University of Technology, Wuhan 430063, China

ARTICLE INFO

Article history:
Received 9 July 2019
Received in revised form
6 November 2019
Accepted 19 December 2019
Available online 30 December 2019

Keywords:
Free vibration
Sound radiation
Transfer matrix method
Cylindrical shell
Variable thickness

ABSTRACT

Based on the Precise Transfer Matrix Method (PTMM), the dynamic model is constructed to observe the vibration behaviour of cylindrical shells with variable thickness by solving a set of first-order differential equations. The free vibration of stiffened cylindrical shells with variable thickness can be obtained to compare with the exact solution and FEM results. The reliability of the present method of free vibration is well proved. Furthermore, the effect of thickness on the vibration responses of the cylindrical shell is also discussed. The acoustic response of immersed cylindrical shells is analyzed by a Pluralized Wave Superposition Method (PWSM). The sound pressure coefficient can be gained by collocating points along the meridian line to satisfy the Neumann boundary condition. The mode convergence analysis of the cylindrical shell is carried out to guarantee calculation precision. Also, the reliability of the present method on sound radiation is verified by comparing with experimental results and numerical results.

1. Introduction

Stiffened cylindrical shells with high compressive strength are widely introduced into engineering structures, especially in the marine field. The radiated noise of submarine which results from structure vibration is a very important issue. Therefore, there are significant theoretical value and engineering meaning to study the vibro-acoustic behaviour of submerged stiffened cylindrical shells. A great number of theoretical researches have been done on the vibration and radiated noise of cylindrical shells. Tottenham and Shimizu (1972) put forward a transfer matrix method to analyze the free vibration characteristics of a cylindrical shell, but the method is hard to analyze the dynamic response of the shell in fluid. Sandman (1976) investigated the acoustic loading and obtained the generalized velocity distribution. The influence of the baffle was observed in the axial pressure variation along the surface. After combining modal superposition with radiation impedance method, Stepanishen (1982) developed an approach to evaluate the vibration and sound radiation of a finite cylindrical shell with infinite rigid baffles in fluid. Both the above models should be modified when the endplates are active radiators. Laulagnet and Guyader (1989) explored the issues of how finite cylindrical shell submerged in light and heavy fluids affected the sound radiation. Under the assumption of rigid baffles on both ends, some researchers also analyze the radiated noise of cylindrical shells. Up to now, there are many analysis methods including wave propagation method (Caresta and Kessissoglou, 2009), modified variational method (Jin et al., 2017), transfer matrix method (Wang et al., 2015), Wittrick-Williams algorithm (El-Kaabazi and Kennedy, 2012) and reverberation-ray matrix (Tang et al., 2017) applied to solve the vibro-acoustic problem of the cylindrical shell. Nevertheless, most of the researchers have been concentrating on cylindrical shells of equal thickness, and there are few applications of variable thickness shells in vibro-acoustic analysis. Obliviously, it's difficult to copy with the fluid load and discontinuity of the stiffened shell.

Considering the complexity of the governing equations of the cylindrical shell, it's hard to obtain the vibration and acoustic response directly of the cylindrical shell with variable thickness by an analytical method. Many numerical methods such as finite element method (Petyt and Lim, 1978), boundary element method (Ventsel et al., 2010) and coupled finite element and boundary element method (Liu and Chen, 2009) have potential advantages to

* Corresponding author. Key Laboratory of High Performance Ship Technology (Wuhan University of Technology), Ministry of Education, Wuhan 430063, China.
E-mail address: xianzhongwang@whut.edu.cn (X. Wang).
Peer review under responsibility of Society of Naval Architects of Korea.

https://doi.org/10.1016/j.ijnaoe.2019.12.003

analyze the dynamic behaviour of arbitrary complex elastic structures. However, the solution accuracy of these numerical methods relies heavily on meshed elements and frequency band.

The aim of the present work is to predict the vibro-acoustic response of immersed stiffened cylindrical shell with variable thickness. After combining a precise transfer matrix method (Wang et al., 2015) and a pluralized wave superposition method (Wang et al., 2016a,b), the authors develop an approach to observe the natural frequencies and radiated noise of cylindrical shells. The convergence analysis of modes (m, n) of the cylindrical shell is carried out to gain the excellent convergence guarantee and calculation precision. The validity and reliability of the present method for predicting free vibration are well proofed by comparing the natural frequencies with analytical results and FEM results.

Furthermore, the effect of variable thickness on the free vibration of the cylindrical shell is discussed. The effectiveness of the present method for evaluating sound radiation of immersed cylindrical shells is also demonstrated by comparing the sound pressure level with experiment results and numerical results.

2. The dynamic model

2.1. The thin shell

A diagrammatic drawing of the stiffened immersed cylindrical shell is shown in Fig. 1. $h(x)$, L, and R denote the thickness, length and height of the cylindrical shell, respectively. A transfer matrix differential equation form of Flügge equations can be obtained

$$d\boldsymbol{Z}(\xi)/d\xi = \mathbf{U}(\xi)\boldsymbol{Z}(\xi) + \boldsymbol{F}(\xi) - \boldsymbol{p}(\xi) \tag{1}$$

where $\mathbf{U}(\xi)$ is the field transfer matrix of the thin shell. The nonzero elements of $\mathbf{U}(\xi)$ can be referred to Wang and Guo (2016). $\mathbf{Z}(\xi) = \{\{\tilde{u} \;\; \tilde{v} \;\; \tilde{w} \;\; \tilde{\psi} \;\; \tilde{M}_s \;\; \tilde{V}_s \;\; \tilde{S}_{s\theta} \;\; \tilde{N}_s\}$. u, v, w, ψ denote the axial, circumferential, radial displacements, angular angle, respectively. $\boldsymbol{F}(\xi)$ and $\boldsymbol{p}(\xi)$ are the dimensionless external force vector and sound pressure load vector. M_s, V_s, $S_{s\theta}$, N_s denote the moment, radial, circumferential and axial forces, respectively. The symbols with over-tilde represent the dimensionless variables. These dimensionless state vectors including four end genetic forces and four displacement functions are

$$(u, w, \psi) = h\sum_{\beta=0}^{1}\sum_{n}(\tilde{u}, \tilde{w}, \tilde{\psi}/R)\sin\left(n\theta + \frac{\alpha\pi}{2}\right), v = h \times \sum_{\beta=0}^{1}\sum_{n}\tilde{v}\cos\left(n\theta + \frac{\alpha\pi}{2}\right) \tag{2a}$$

$$(N_s, V_s, M_s) = \frac{K}{R^2}\sum_{\beta=0}^{1}\sum_{n}(\tilde{N}_s, \tilde{V}_s, \tilde{M}_s R)\sin\left(n\theta + \frac{\alpha\pi}{2}\right), S_{s\theta} = \frac{K}{R^2}\sum_{\beta=0}^{1}\sum_{n}\tilde{S}_{s\theta}\cos\left(n\theta + \frac{\alpha\pi}{2}\right) \tag{2b}$$

where $\alpha = 1$ denotes the symmetric mode, $\alpha = 0$ denotes the anti-symmetric mode. Bending rigidity K equals $Eh^3/12(1-\nu^2)$, and E, ν, h are Young's modulus, Poisson's ratio and thickness of the shell respectively.

2.2. The ring-stiffener

The vibration of the stiffener could result in four kinds of forms of vibration of the shell, two of which are movements within the plane, namely flexural and extending vibration within the plane, and the other are flexural and torsional movements out of the plane. The ring-stiffeners are laid on the internal surface of the shell. If the kth stiffener and the cylindrical shell are welded together at a position ξ_k, there are differences of internal forces between the state vector $\boldsymbol{Z}(\xi_k^L)$ at the left end ξ_k^L and the state vector $\boldsymbol{Z}(\xi_k^R)$ at the right end ξ_k^R. The state vector $\boldsymbol{Z}(\xi_k)$ satisfies

$$\boldsymbol{Z}\left(\xi_k^R\right) = \boldsymbol{T}r_k\boldsymbol{Z}\left(\xi_k^L\right) \tag{3}$$

where $\boldsymbol{Z}(\xi_k^L)$ and $\boldsymbol{Z}(\xi_k^R)$ denote state vectors of both ends,

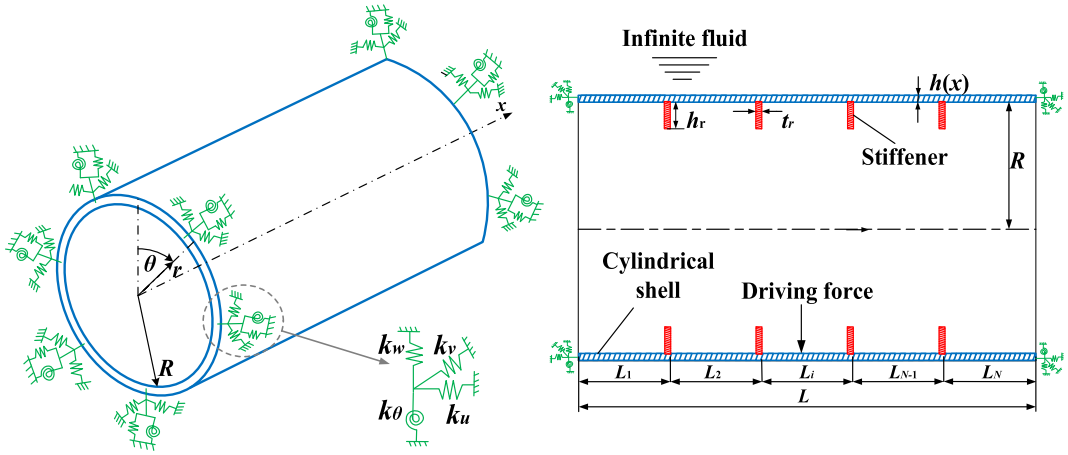

Fig. 1. Scheme for the immersed stiffened cylindrical shell.

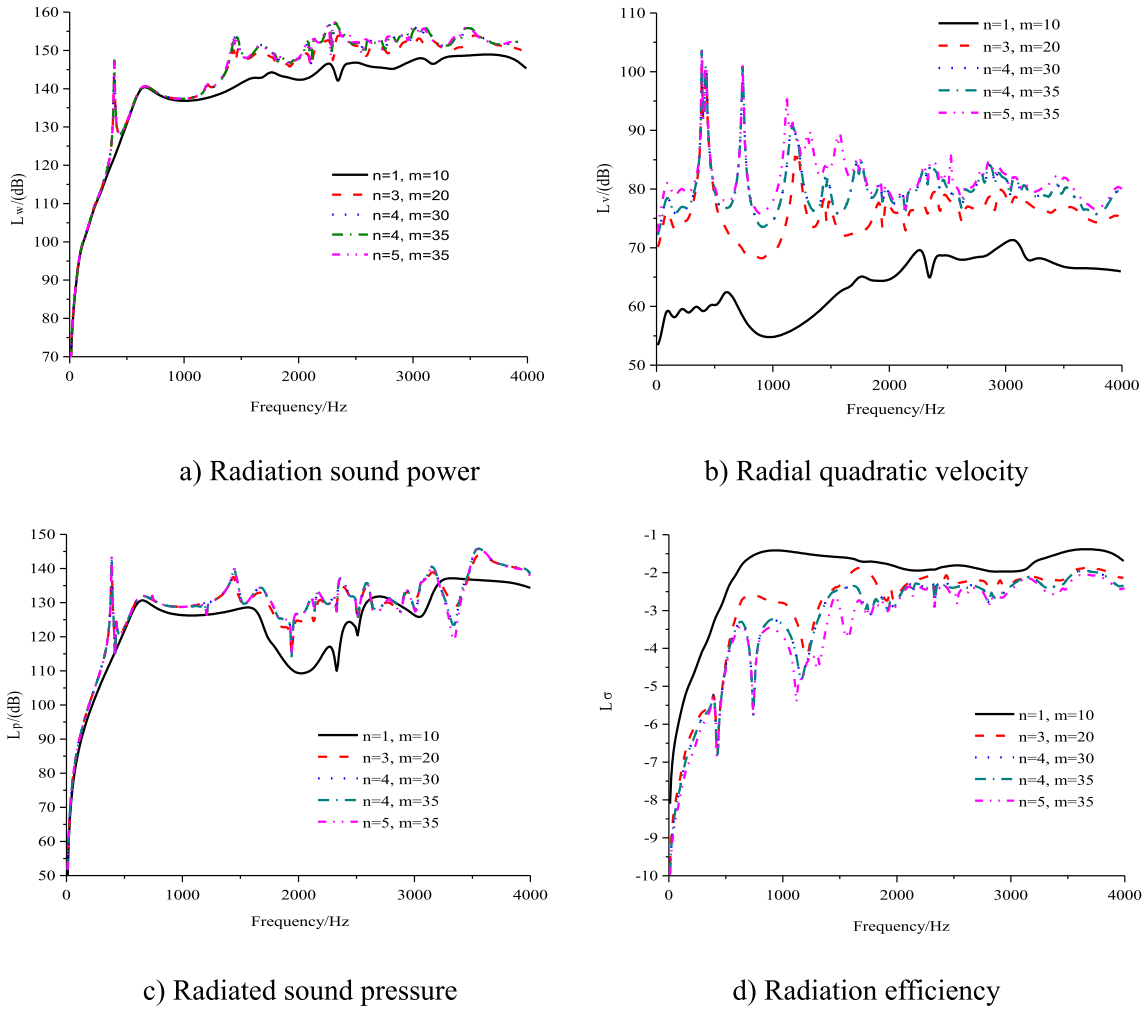

Fig. 2. Convergence analysis of mode (m, n) on the vibro-acoustic response.

respectively. The effect of the ring-stiffener plate is considered only to change the transfer relation of state vectors at the left and right ends of the action point. Hence, $\boldsymbol{T}r_k$ is obtained in a point transfer matrix form, the nonzero elements of which is given in Appendix A.

2.3. The added mass

The position of the ith added mass in the shell is located at (x_{0i}, θ_{0i}), $i = 1,2, \ldots,N$, the mass of which is m_i. By dealing with the ith added mass $m_i\delta(x_{0i})\delta(\theta_{0i})$ with an orthogonal transformation, one obtains

Table 1
Comparison of natural frequencies of the cylindrical shell in vacuo (unit:Hz).

	n = 0			n = 1		
	Present method	Exact solution	Error	Present method	Exact solution	Error
m = 1	8011.2	8011.06	0.00%	4944.0	4943.79	0.00%
m = 2	8205.4	8204.57	−0.01%	7309.7	7308.55	−0.02%
m = 3	8288.3	8286.39	−0.02%	7910.6	7908.31	−0.03%
m = 4	8453.6	8450.23	−0.04%	8256.5	8252.68	−0.05%
m = 5	8780.3	8775.06	−0.06%	8670.0	8664.38	−0.06%
m = 6	9341.2	9334.10	−0.08%	9281.6	9274.18	−0.08%
	n = 2			n = 3		
	Present method	Exact solution	Error	Present method	Exact solution	Error
m = 1	2835.5	2833.37	−0.08%	1749.2	1741.54	−0.44%
m = 2	5664.3	5661.85	−0.04%	4243.4	4237.93	−0.13%
m = 3	6998.5	6994.89	−0.05%	5951.6	5945.51	−0.10%
m = 4	7737.3	7732.17	−0.07%	7062.8	7055.49	−0.10%
m = 5	8370.5	8363.75	−0.08%	7962.9	7954.11	−0.11%
m = 6	9119.3	9110.79	−0.09%	8898.5	8888.28	−0.11%

Table 2
Comparison of natural frequencies of the immersed cylindrical shell (unit:Hz).

	Present method	Wave propagation method	FEM	Error
(1,2)	4.94	4.92	4.95	0.41%
(1,3)	8.91	9.06	8.95	1.66%
(2,2)	10.86	10.71	10.66	1.40%
(2,3)	11.56	11.24	11.54	2.85%
(3,3)	14.68	14.7	14.73	0.14%
(1,4)	18.24	18.68	18.26	2.36%
(2,4)	18.68	19.14	18.71	2.40%
(3,4)	20.14	20.37	20	1.13%

Table 3
Comparison of natural frequencies of the cylindrical shell with variable thickness (unit:Hz).

		$m=1$	$m=2$	$m=3$	$m=4$	$m=5$
Present method	$n=0$	7971.49	8222.84	8371.82	8708.67	9367.78
	$n=1$	5448.93	7326.32	8007.15	8529.87	9281.85
	$n=2$	2799.47	5699.95	7135.97	8073.98	9060.99
	$n=3$	1826.50	4351.26	6180.04	7518.60	8795.40
	$n=4$	1679.89	3568.28	5451.98	7055.56	8594.51
FEM	$n=0$	7971.30	8164.00	8302.30	8625.60	9271.00
	$n=1$	5416.20	7277.90	7944.50	8452.00	9189.00
	$n=2$	2782.70	5665.50	7086.60	8007.90	8977.60
	$n=3$	1803.50	4321.20	6139.30	7462.70	8720.80
	$n=4$	1641.40	3531.20	5409.60	7001.30	8521.80
Error	$n=0$	0.00%	0.72%	0.84%	0.96%	1.04%
	$n=1$	0.60%	0.67%	0.79%	0.92%	1.01%
	$n=2$	0.60%	0.61%	0.70%	0.83%	0.93%
	$n=3$	1.28%	0.70%	0.66%	0.75%	0.86%
	$n=4$	2.34%	1.05%	0.78%	0.78%	0.85%

$$m(x_i,\theta_i)=\delta(x_{0i})\sum_{\alpha=0}^{1}\sum_{n=0}^{\infty}m_{ni}\sin\left(n\theta+\frac{\alpha\pi}{2}\right) \tag{4}$$

where $m_{ni}=m_0\frac{\varepsilon_n}{2\pi}\sin\left(n\theta_0+\frac{\alpha\pi}{2}\right)$, $\varepsilon_n=\begin{cases}1, n=0\\ 2, n\neq 0\end{cases}$.

There are differences $m_{ni}\omega^2X(X=u,v,w,\psi)$ between the state vector $\boldsymbol{Z}(\xi_s^L)$ and the state vector $\boldsymbol{Z}(\xi_s^R)$ at a position $\xi_s=x_{0i}/R$. The state vector $\boldsymbol{Z}(\xi_s)$ satisfies

$$\boldsymbol{Z}\left(\xi_s^R\right)=\boldsymbol{P}_{ni}\boldsymbol{Z}\left(\xi_s^L\right) \tag{5}$$

where $\boldsymbol{Z}(\xi_k^L)$ and $\boldsymbol{Z}(\xi_k^R)$ denote state vectors at the left end ξ_s^L and the right end ξ_s^R, respectively. $\boldsymbol{P}_{ni}$ is the point transfer matrix of ith added mass.

2.4. The exciting force

A concentrated force $f(x,\theta)$ is introduced to act on the point (x_0, θ_0) of the stiffener or the shell. An orthogonal transformation is carried out to deal with the formula $f(x,\theta)=f_0\delta(x_0)\delta(\theta_0)$. After multiplying the formula by $\sum_{p=0}^{\infty}\sin\left(p\theta+\frac{\alpha\pi}{2}\right)\sin\left(n\theta+\frac{\alpha\pi}{2}\right)$ and integrating from 0 to 2π, one obtains

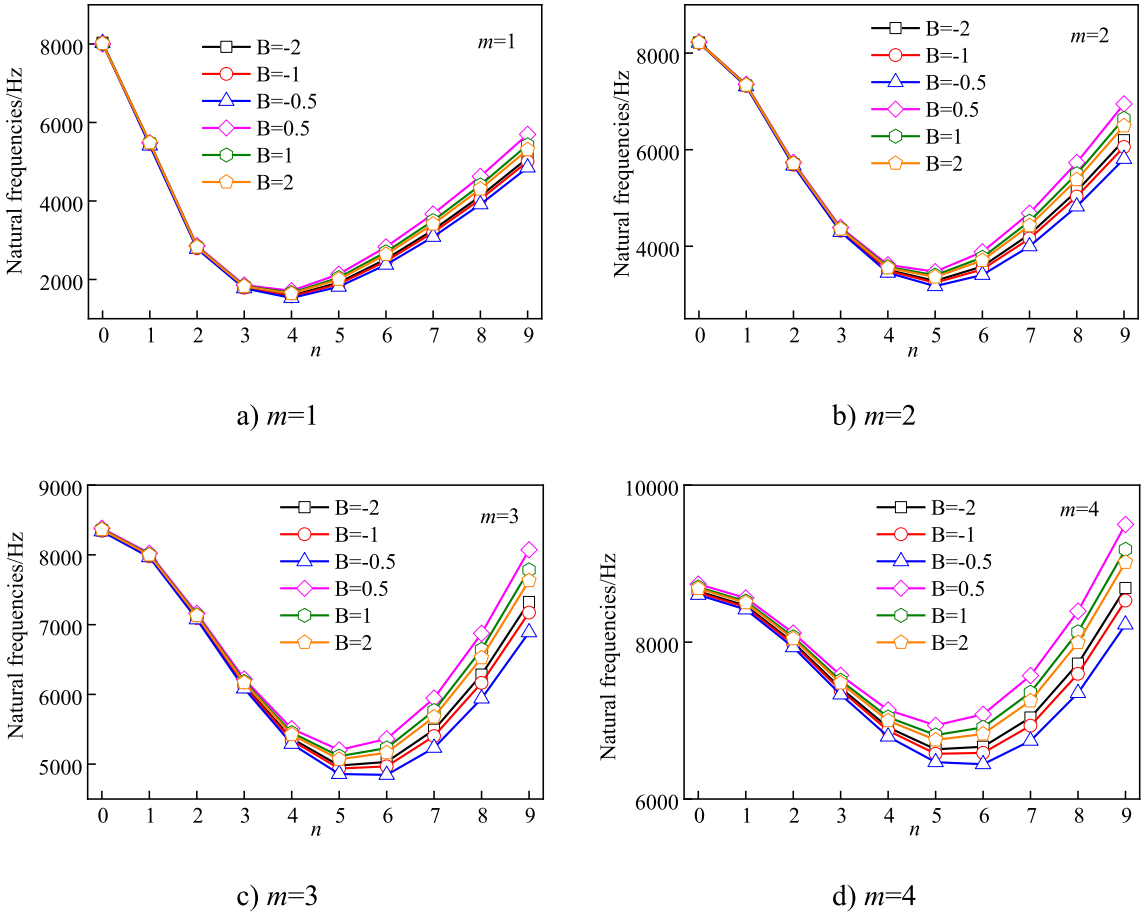

Fig. 3. Variations of natural frequencies of the cylindrical shell with various coefficient B.

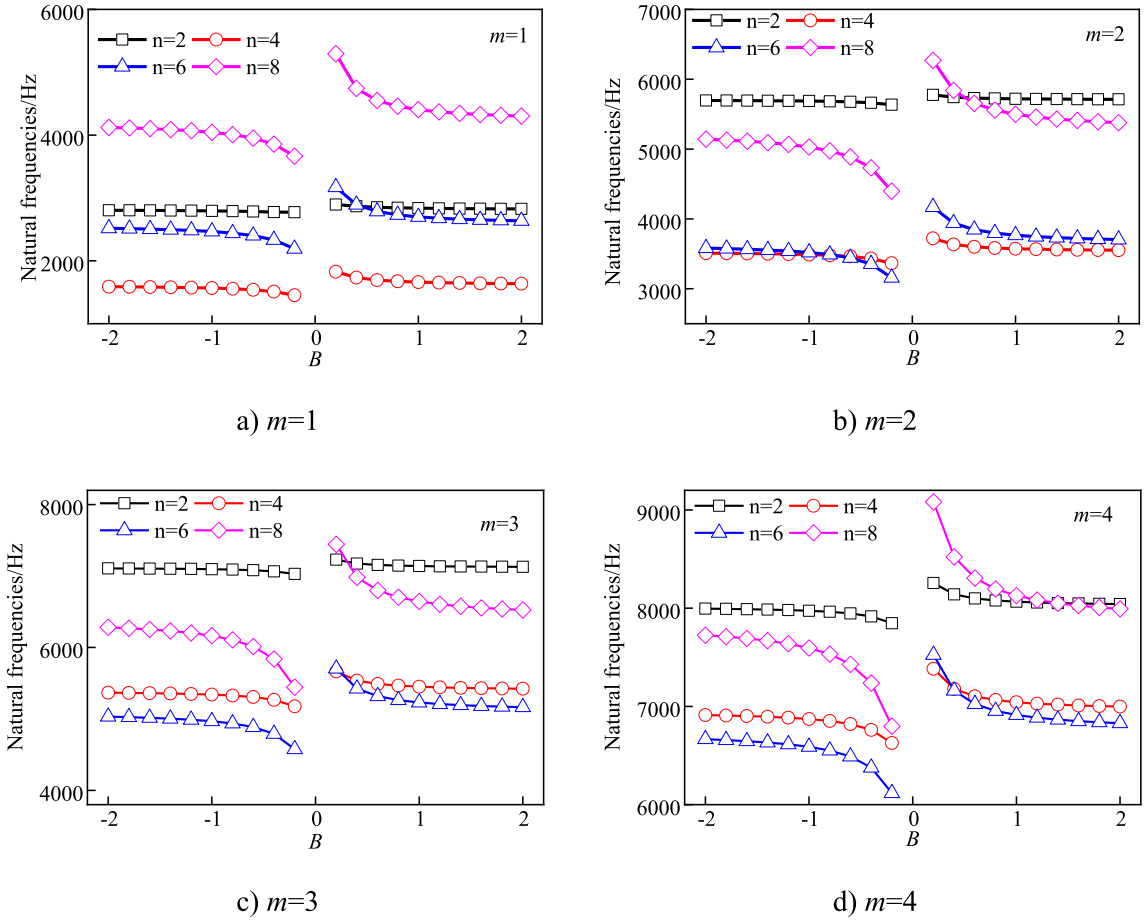

Fig. 4. Variations of natural frequencies of the cylindrical shell versus the coefficient *B*.

$$f(x,\theta)=\delta(x_0)\sum_{\alpha=0}^{1}\sum_{n=0}^{\infty}f_n\sin\left(n\theta+\frac{\alpha\pi}{2}\right) \tag{6}$$

where $f_n=f_0\frac{\varepsilon_n}{2\pi}\sin\left(n\theta_0+\frac{\alpha\pi}{2}\right)$, $\varepsilon_n=\begin{cases}1, n=0\\ 2, n\neq 0\end{cases}$.

2.5. The vibrational responses

Case I. If there is no ring rib and added mass in the *j*th segment ($\xi_j \sim \xi_{j+1}$), the relation between $\boldsymbol{Z}(\xi_j)$ and $\boldsymbol{Z}(\xi_{j+1})$ can be constructed as

$$\boldsymbol{Z}(\xi_{j+1})=\exp[\boldsymbol{U}(\xi_{j+1}-\xi_j)]\boldsymbol{Z}(\xi_j)+\int_{\xi_j}^{\xi_{j+1}}\exp[\boldsymbol{U}(\xi_{j+1}-\tau)]\boldsymbol{r}(\tau)d\tau \tag{7}$$

Case II. If there is a ring rib located in the *j*th segment ($\xi_j \sim \xi_{j+1}$), the relation between $\boldsymbol{Z}(\xi_j)$ and $\boldsymbol{Z}(\xi_{j+1})$ can be constructed as

$$\boldsymbol{Z}(\xi_{j+1})=e^{\int_{\xi_i}^{\xi_{j+1}}\boldsymbol{U}(\tau)d\tau}\boldsymbol{T}\boldsymbol{r}_i\left(e^{\int_{\xi_j}^{\xi_i}\boldsymbol{U}(\tau)d\tau}\boldsymbol{Z}(\xi_j)+\int_{\xi_j}^{\xi_i}e^{\int_{\tau}^{\xi_i}\boldsymbol{U}(s)ds}\boldsymbol{f}(\tau)d\tau\right)+\int_{\xi_i}^{\xi_{j+1}}e^{\int_{\tau}^{\xi_{j+1}}\boldsymbol{U}(s)ds}\boldsymbol{f}(\tau)d\tau \tag{8}$$

Case III. If there is an added mass located in the *j*th segment ($\xi_j \sim \xi_{j+1}$), the relation between $\boldsymbol{Z}(\xi_j)$ and $\boldsymbol{Z}(\xi_{j+1})$ can be constructed as

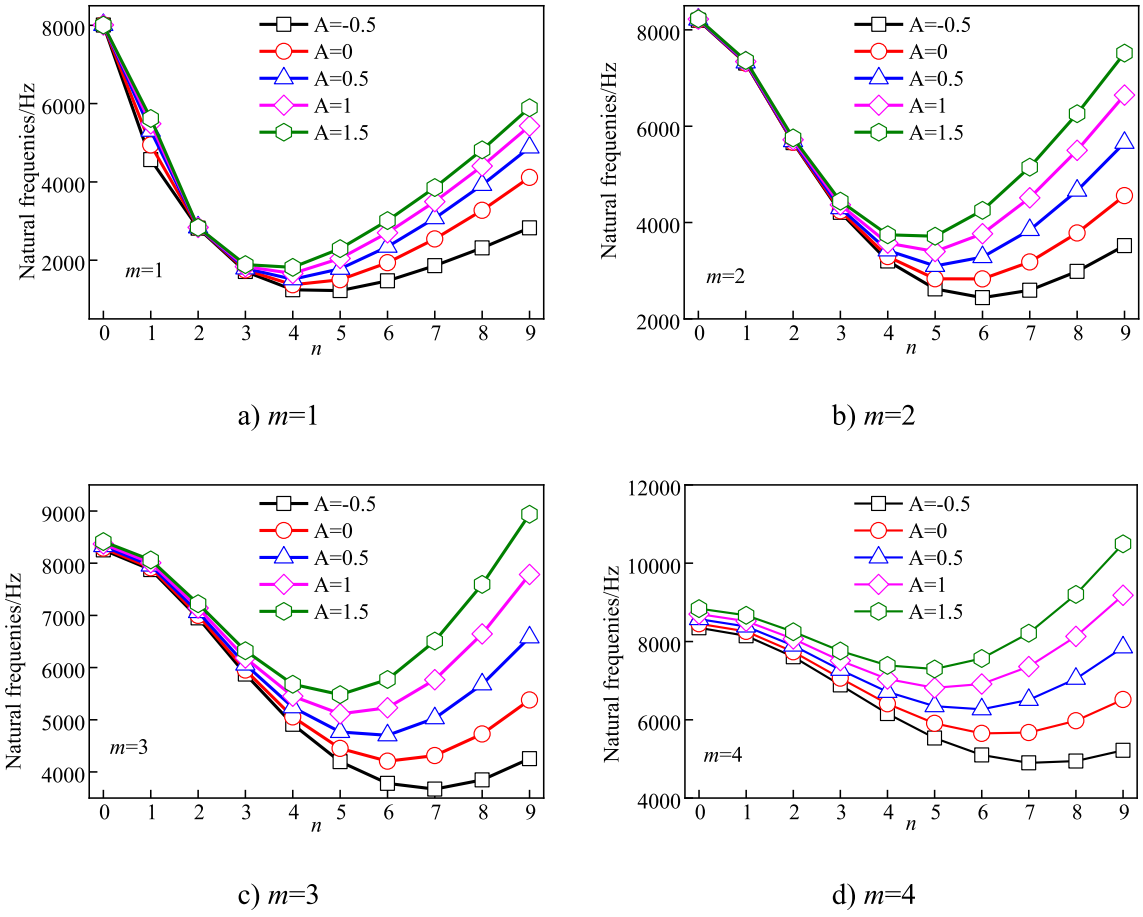

Fig. 5. Variations of natural frequencies of the cylindrical shell with various coefficient A.

$$\boldsymbol{Z}(\xi_{j+1}) = e^{\int_{\xi_i}^{\xi_{j+1}} \boldsymbol{U}(\tau)d\tau} \boldsymbol{P}_{ni}\left(e^{\int_{\xi_j}^{\xi_i} \boldsymbol{U}(\tau)d\tau} \boldsymbol{Z}(\xi_j) + \int_{\xi_j}^{\xi_i} e^{\int_{\tau}^{\xi_i} \boldsymbol{U}(s)ds} \boldsymbol{f}(\tau)d\tau\right) + \int_{\xi_i}^{\xi_{j+1}} e^{\int_{\tau}^{\xi_{j+1}} \boldsymbol{U}(s)ds} \boldsymbol{f}(\tau)d\tau \tag{9}$$

The relation between $\boldsymbol{Z}(\xi_j)$ and $\boldsymbol{Z}(\xi_{j+1})$ can be simplified as

$$\boldsymbol{Z}(\xi_{j+1}) = \boldsymbol{T}_{j+1}\boldsymbol{Z}(\xi_j) + \boldsymbol{P}_{j+1},\ j = 1, \ldots, N-1 \tag{10}$$

where $\boldsymbol{T}_{j+1} = e^{\int_{\xi_j}^{\xi_{j+1}} \boldsymbol{U}(\tau)d\tau}$, $\boldsymbol{P}_{j+1} = \int_{\xi_j}^{\xi_{j+1}} e^{[\boldsymbol{U}(\xi_{j+1}-\tau)]}\boldsymbol{r}(\tau)d\tau$ in Case I; $\boldsymbol{T}_{j+1} = -e^{\int_{\xi_i}^{\xi_{j+1}} \boldsymbol{U}(\tau)d\tau}\boldsymbol{T}\boldsymbol{r}_i e^{\int_{\xi_j}^{\xi_i} \boldsymbol{U}(\tau)d\tau}$, $\boldsymbol{P}_{j+1} = e^{\int_{\xi_i}^{\xi_{j+1}} \boldsymbol{U}(\tau)d\tau}\boldsymbol{T}\boldsymbol{r}_i \int_{\xi_j}^{\xi_i} e^{\int_{\tau}^{\xi_i} \boldsymbol{U}(s)ds}\boldsymbol{f}(\tau)d\tau + \int_{\xi_i}^{\xi_{j+1}} e^{\int_{\tau}^{\xi_{j+1}} \boldsymbol{U}(s)ds}\boldsymbol{f}(\tau)d\tau$ in Case II; $\boldsymbol{T}_{j+1} = -e^{\int_{\xi_i}^{\xi_{j+1}} \boldsymbol{U}(\tau)d\tau}\boldsymbol{P}_{ni} e^{\int_{\xi_j}^{\xi_i} \boldsymbol{U}(\tau)d\tau}$, $\boldsymbol{P}_{j+1} = e^{\int_{\xi_i}^{\xi_{j+1}} \boldsymbol{U}(\tau)d\tau}\boldsymbol{P}_{ni} \int_{\xi_j}^{\xi_i} e^{\int_{\tau}^{\xi_i} \boldsymbol{U}(s)ds}\boldsymbol{f}(\tau)d\tau + \int_{\xi_i}^{\xi_{j+1}} e^{\int_{\tau}^{\xi_{j+1}} \boldsymbol{U}(s)ds}\boldsymbol{f}(\tau)d\tau$ in Case III.

According to the ideas of finite element assembling mass matrix and rigidity matrix, Eq. (10) is assembled and the equations of the whole structure can be transferred into

$$\begin{bmatrix} -\boldsymbol{T}_2 & \boldsymbol{I}_8 & 0 & 0 & 0 & 0 \\ 0 & -\boldsymbol{T}_3 & \boldsymbol{I}_8 & 0 & 0 & 0 \\ 0 & 0 & -\boldsymbol{T}_4 & \boldsymbol{I}_8 & 0 & 0 \\ 0 & 0 & 0 & \ldots & \boldsymbol{I}_8 & 0 \\ 0 & 0 & 0 & 0 & -\boldsymbol{T}_N & \boldsymbol{I}_8 \end{bmatrix} \begin{Bmatrix} \boldsymbol{Z}(\xi_1) \\ \boldsymbol{Z}(\xi_2) \\ \boldsymbol{Z}(\xi_3) \\ \vdots \\ \boldsymbol{Z}(\xi_N) \end{Bmatrix} = \begin{Bmatrix} \boldsymbol{P}_2 \\ \boldsymbol{P}_3 \\ \boldsymbol{P}_4 \\ \vdots \\ \boldsymbol{P}_N \end{Bmatrix} \tag{11}$$

Constrained stiffness constants k_u, k_v, k_w and k_θ are employed to restrain displacements in the axial, tangential, radial and rotational directions at both ends of the cylindrical shell. The dimensionless internal forces and displacements at both ends satisfy the relationship

$$\tilde{M}_x = \tilde{k}_\theta\tilde{\phi},\ \tilde{S}_{x\theta} = \tilde{k}_w\tilde{w},\ \tilde{V}_x = \tilde{k}_v\tilde{v},\ \tilde{N}_x = \tilde{k}_u\tilde{u} \tag{12}$$

where $\tilde{k}_s = k_s R^2 h/K$, $s = u, v, w, \theta$ are dimensionless stiffness coefficients. Classic boundary conditions including S (Simply-support), C (Clamped) and F (Free) are special cases of E (Elastic restrain) boundary conditions. When the dimensionless stiffness coefficients are generally taken as 10^6, the displacement result at the end tends to be zero which is approximately equivalent to the clamped boundary. The not restrained displacement is Free boundary if the dimensionless stiffness coefficient is set as 0. By identifying the line numbers of the determinate state vectors in $\boldsymbol{Z}(\xi_1)$, $\boldsymbol{Z}(\xi_N)$, deleting the corresponding row and column in the coefficient matrix in Eq. (11) and expanding the coefficient matrix

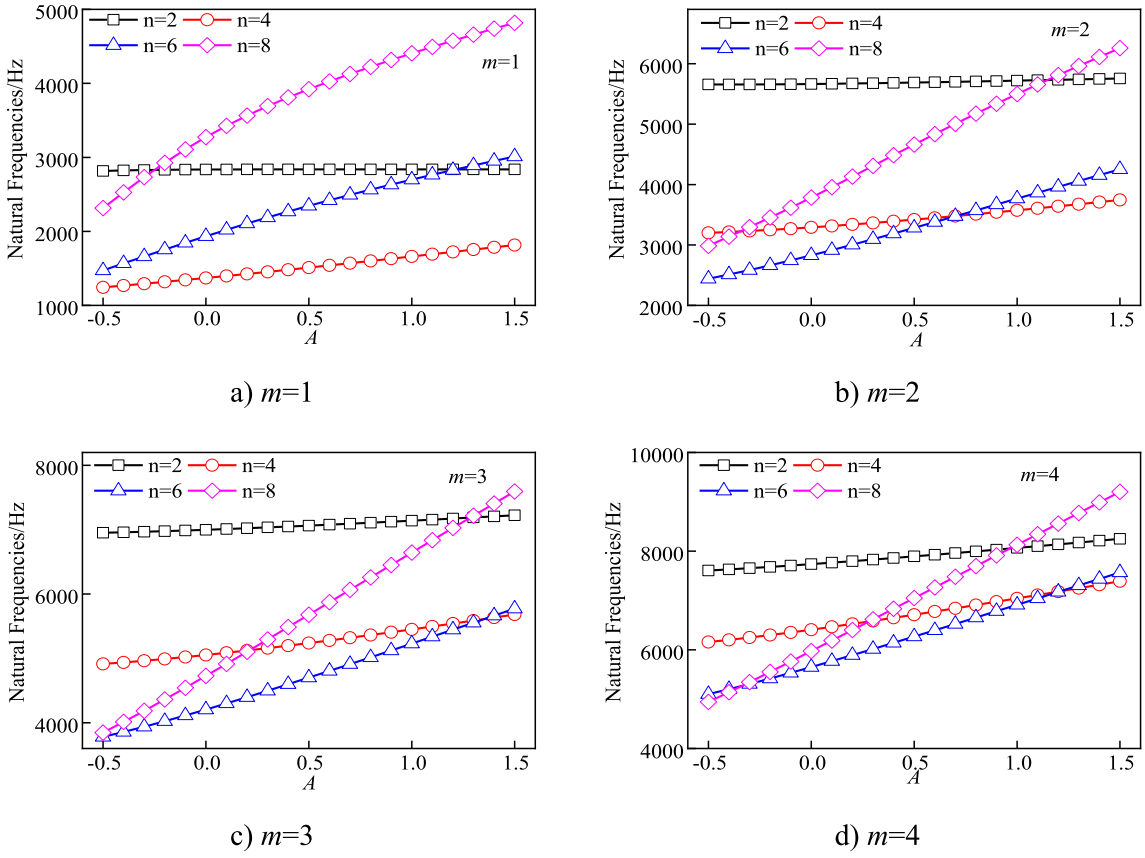

Fig. 6. Variations of natural frequencies of the cylindrical shell versus the coefficient A.

determinant, the dispersion equation of the cylindrical shell can be constructed to gain the natural frequencies of the stiffened cylindrical shell.

2.6. The acoustic responses

A virtual interior surface S' is constructed with virtual sources by shrinking the real surface S. The fluid load p is expressed as:

$$p(P) = \iint_{S'} \sigma(O) K(P,O) dS' \tag{13}$$

where P and O denote the external field point and source point, respectively. $\sigma(O)$ denotes the unknown distribution function of the virtual source strength density. The source strength function $K(P,O)$ and the distribution function $\sigma(O)$ can be expanded into a complex Fourier series. The distance $d(P,O)$ equals $\sqrt{r_P^2 + r_O^2 - 2r_P r_O \cos(\theta_P - \theta_O) + (z_P - z_O)^2}$. A complex distance $\overline{d}$ satisfying $(1+i\gamma)d$ is employed to avoid the non-uniqueness solution at certain characteristic frequencies. The integral interval

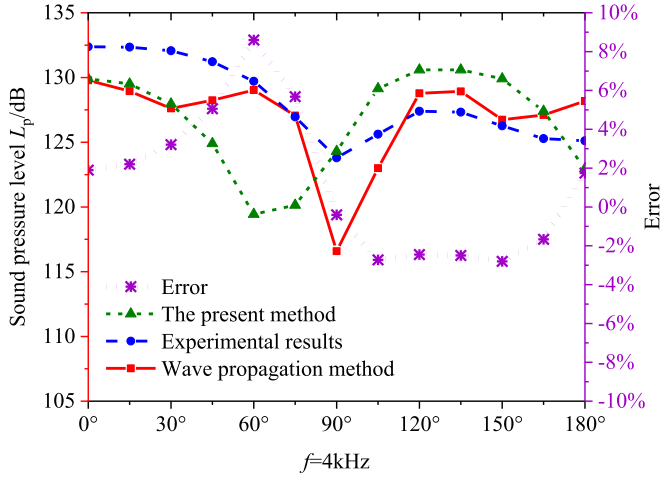

Fig. 7. Comparison of sound pressure level of Model IV.

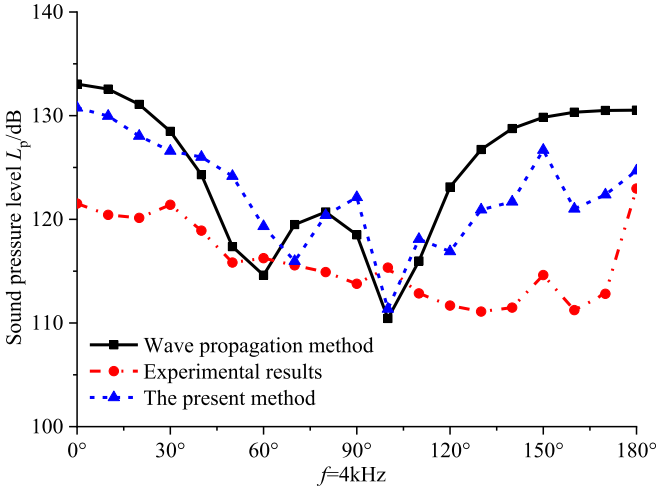

Fig. 8. Comparison of sound pressure level of Model V.

$(0\tilde{}L')$ and the integral interval $(0\tilde{}2\pi)$ are divided into M and N equal divisions respectively, Eq. (13) yields

$$p(P)=\sum_{n=-\infty}^{+\infty}\sum_{m=-\infty}^{+\infty}c_{mn}K_{mn}(\tilde{P})e^{in\theta_p} \tag{14}$$

where $K_{mn}(\tilde{P})=\frac{2\pi L'}{MN}\sum_{k_1=0}^{M-1}\sum_{k_2=0}^{N-1}K[\tilde{P},k_1,k_2]r_{L_0}e^{imk_1\frac{2\pi}{M}}e^{-ink_2\frac{2\pi}{N}}$ is the generalized sound pressure load. L' denotes the meridian line length of the virtual source surface. $K_{mn}(\tilde{P})$ can be obtained by the discrete Fourier transform method quickly and accurately.

By expanding the potential function into a complex Fourier series, the normal derivative of fluid load p is expressed as

$$\frac{\partial p(P)}{\partial n_P}=\sum_{n=-\infty}^{+\infty}\sum_{m=-\infty}^{+\infty}c_{mn}K'_{mn}(\tilde{P},\tilde{O})e^{in\theta_p} \tag{15}$$

The whole points (ξ_i, $i=1, 2, \ldots, m$) on the meridian line of real surface S should satisfy the Neumann boundary condition, which yields

$$\boldsymbol{K}'_n\boldsymbol{c}_n=\rho_0\omega^2\boldsymbol{w}_n,\ n\in(-\infty\tilde{}+\infty) \tag{16}$$

where $\boldsymbol{w}_n=\{w_n(\xi_1)\ \cdots\ w_n(\xi_{m-1})\ w_n(\xi_m)\}^T$ and $\boldsymbol{c}_n=\{c_{-m,n}\ \cdots\ c_{m-1,n}\ c_{mn}\}^T$. ρ_0 denotes the density of the fluid media. ω denotes the circular frequency.

The radial displacement w satisfying the linear superposition principle, one can get

$$w_n(\tilde{P})=w_n^f(\tilde{P})+\sum_{m=-\infty}^{+\infty}c_{mn}w_{mn}^p(\tilde{P}) \tag{17}$$

where $w_n^f(\tilde{P})$ denotes the radial displacement under the external load $\boldsymbol{F}(\xi)$. $w_{mn}^p(\xi)$ denotes the radial displacement under generalized sound pressure load K_{mn}.

After collocating points $\tilde{P}$ on the meridian line of the surface S and substituting Eq. (17) into Eq. (16), one can get

$$\boldsymbol{U}_n\boldsymbol{c}_n=\boldsymbol{Q}_n,\ n\in(-\infty\tilde{}+\infty) \tag{18}$$

where $\boldsymbol{U}_{q\times 2m+1}=K'_{mn}(\tilde{P})-\rho_0\omega^2w_{mn}^p(\tilde{P})$, $\boldsymbol{Q}_{q\times 1}=\rho_0\omega^2w_n^f(\tilde{P})$. Moore-Penrose generalized inverse method is employed to solve the unknown coefficient vector $\boldsymbol{c}_n$. Then the radiated noise of immersed cylindrical shells is obtained by the pluralized wave superposition method (PWSM).

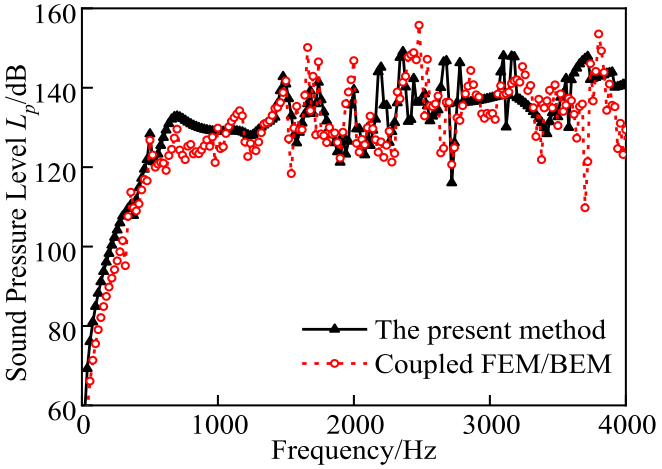

Fig. 9. Comparison of sound pressure level of Model VI.

3. Results

3.1. Convergence analysis

The convergence of numerical results involves the intercepting mode error. The geometric parameters of a simply-supported cylindrical shell are given as follows: radius $R=0.2$ m, length $L=0.6$ m, thickness $h=3$ mm, size of the internal stiffener is 2 mm × 30 mm, stiffener interval is 0.2 m. The radial unit force acts on the position ($L/20^o$, 0.2 m) (cylindrical coordinate) of the internal surface. The measuring point is located at the position ($L/20^o$, 1.2 m). The frequency domain is 40~4 kHz and the frequency step is 40 Hz. The shell and stiffener are made of steel, with density $\rho=7850$ kg/m^3, Poisson's ratio $\mu=0.3$, Young's modulus of elasticity $E=2.06\times10^{11}$ Pa, and damping loss factor $\eta=0.01$. The sound speed of the fluid $c_0=1500$ m/s and the density $\rho_0=1000$ kg/m^3.

As shown in Fig. 2, a convergence is brought about with few modes in low frequency range. More modes are employed to ensure high accuracy as the frequency increases. The number of axial wavenumber m and circumferential wavenumber n take 0–5 and 1–35 respectively in order to realize the accuracy guarantee in the calculated frequency range.

3.2. The free vibration

a) Comparison: Model I

In order to prove the effectiveness of the present method, the geometric and physical parameters of the cylindrical shell (Model I) with simply supported boundary conditions are given as follows: radius $R=0.1$ m, length $L=0.2$ m, thickness $h=2$ mm, density $\rho=7850$ kg/m^3, Poisson's ratio $\mu=0.3$ and Young's modulus of elasticity $E=2.1\times10^{11}$ Pa. The natural frequencies for each order (m, n) are calculated and compared with the exact solution as shown in Table 1. The natural frequencies obtained by the present method are basically consistent with the exact solution. The maximum relative errors are no more than 0.5%, which demonstrates the reliability of the present method on free vibration of the cylindrical shell.

b) Comparison: Model II

The emphasis of this part is to fully verify the effectiveness of the present method on natural frequencies of the submerged cylindrical shell. The geometric and physical parameters of the model II (Zhang, 2002) are given as follows: radius $R=1.0$ m, length $L=20$ m, thickness $h=10$ mm, Poisson's ratio $\mu=0.3$, Young's modulus of elasticity $E=2.1\times1011$ Pa and density $\rho=7850$ kg/m^3. Sound speed c_0 in water equals 1500 m/s. The density of water $\rho_0=1000$ kg/m^3. For a clamped cylindrical shell, the natural frequencies of the immersed shell are compared with analytical results and FEM result, as shown in Table 2. The maximum relative error is no more than 3%, which shows that the present method is consistent with FEM results and wave propagation method. It also demonstrates the reliability of the present method on free vibration of the immersed cylindrical shell.

c) Comparison: Model III

Model III is constructed to validate the reliability of the method on free vibration of the cylindrical shell with variable thickness. The

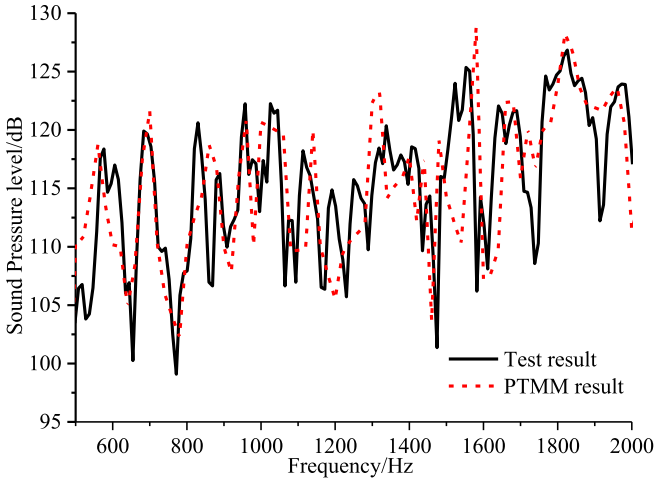

(a)

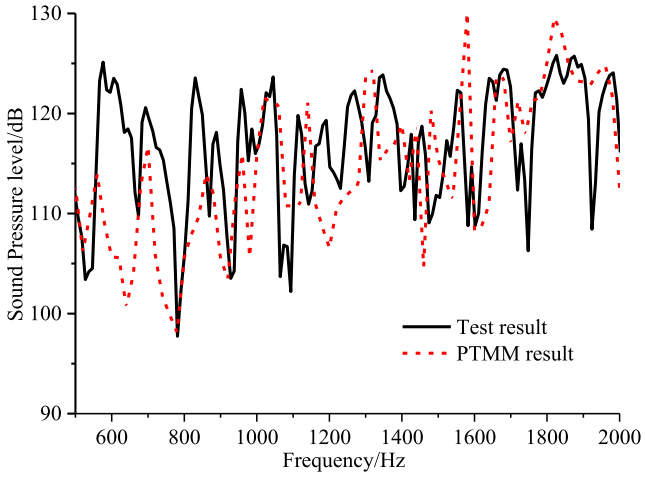

(b)

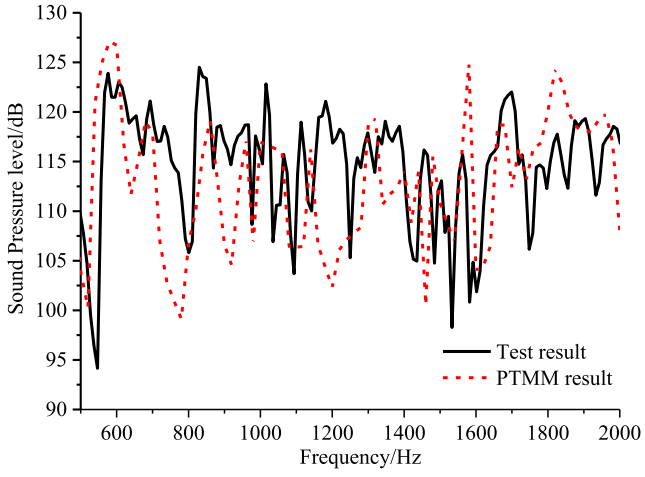

(c)

Fig. 10. Comparison of sound pressure level of Model Ⅶ: (a) hydrophone 1, (b) hydrophone 2, (c) hydrophone 3.

geometric and physical parameters of the Model III are given as follows: radius $R = 0.1$ m, length $L = 0.2$ m, Poisson's ratio $\mu = 0.3$, Young's modulus of elasticity $E = 2.1 \times 10^{11}$ Pa and density $\rho = 7800$ kg/m^3. The thickness h equals $h_0(1 + Ax/L)^B$, which is the function of the axial coordinate value x. Both A and B are suggested to be 1. h_0 is set to 2 mm. The natural frequencies of the simply supported cylindrical shell with variable thickness are compared with FEM results, as shown in Table 3. From Table 3, the natural frequencies obtained by the present method are in good agreement with FEM results. The maximum relative difference is no more than 3%.

To keep both the thickness of both ends to be constant (the thickness of left end $h_l = 2$ mm and the thickness of right end $h_r = 4$ mm), the model III was employed to analyze the influence of thickness coefficient A and B on free vibration of the cylindrical shell with various thickness. When circumferential wavenumber n is 2, 4, 6 and 8 respectively, the relation between natural frequencies and thickness coefficient B was analyzed, as shown in Fig. 3 and Fig. 4. The effect of the thickness coefficient B can be ignored when circumferential wavenumber n is less than 4. The difference becomes more obvious as the circumferential wavenumber n and axial wavenumber m increase. For a given wavenumber n, the curve shows the antisymmetric characteristic. When the thickness coefficient B is negative, the natural frequency goes up as the thickness coefficient B increases. It comes to an opposite conclusion when the thickness coefficient B is positive.

When circumferential wavenumber n was 2, 4, 6 and 8 respectively, the relation between natural frequencies and thickness coefficient A was also analyzed, as shown in Fig. 5 and Fig. 6. The effect of the thickness coefficient A is in accordance with that of the thickness coefficient B when circumferential wavenumber n is less than 4. The only difference is that the coefficient A affects the natural frequency when $m = 1$ and $n = 1$. The difference of natural frequencies become more obvious as the circumferential wavenumber n and axial wavenumber m increase. The natural frequency goes up as the thickness coefficient A increases when $n = 4$, 6 and 8. When $n = 2$ the curve is approximately a horizontal line, which means thickness coefficient A has little impact on the natural frequency.

3.3. The acoustic response

a) Comparison analysis: Model Ⅳ

The geometric parameters of the Model Ⅳ are given as follows: radius $R = 0.175$ m, length $L = 0.6$ m, thickness $h = 2$ mm. The centre of the left end of the cylindrical shell was defined cylindrical coordinate origin. The radial unit force acts on the point (L/2,0°,0.175) (cylindrical coordinates) of the cylindrical shell with excitation frequency $f = 4$ kHz. The hydrophone is fixed at the position of 1 m from the external surface of the shell. The physical parameters of the shell are given as follows: Poisson's ratio $\mu = 0.3$, Young's modulus of elasticity $E = 2.1 \times 1011$ Pa, density $\rho = 7850$ kg/m3, and loss factor $\eta = 0.01$. Sound speed c_0 in water equals 1500 m/s. The density of water $\rho_0 = 1000$ kg/m^3. The simply supported boundary conditions at both ends are assumed. The results contrast of sound pressure level L_p is yielded by adopting the present method, experimental method and B. Laulgnet's method respectively, as shown in Fig. 7. The error curve shows the maximum error of the sound pressure level between the present method and experiment results. It can be seen from Fig. 7 that the error of sound pressure level is 0.5%–5% at other angles except at 60°, which accords with the allowable range of error. It proves that the present method is feasible, effective and sufficiently accurate

and can be applied to predict sound radiation of cylindrical shells.

b) Comparison analysis: Model V

The geometric parameters of the Model V with simply supported boundary condition are given as follows: radius $R = 0.2$ m, length $L = 0.6$ m, thickness $h = 3$ mm. Sectional dimensions of the stiffener is 2 mm × 30 mm. The stiffeners spacing $\Delta l = 0.2$ m. The radial unit force acts on the point (0.3 m, 0°, 0.2 m) (cylindrical coordinates) of the shell with excitation frequency $f = 4$ kHz. The hydrophone is fixed at the position of 1 m from the external surface of the shell. The physical parameters are the same as model IV. It can be seen from Fig. 8 that the relative error of sound pressure level between the present method and wave propagation method is no more than 6%. The results from the present method also are consistent with the experimental values, except for some minor differences in some partial angle. Hence, the present method proposed can be applied to vibro-acoustic behaviour of the stiffened cylindrical shell.

c) Comparison analysis: Model VI

Model VI with the variable thickness is constructed to validate the availability and accuracy of the present method on the sound radiation of the cylindrical shell with the variable thickness. The geometric and physical parameters of the Model VI with clamped boundary condition are given as follows: the variation coefficient $A = 1$, the power coefficient $B = 1$. The other geometric and physical parameters are the same as model V, except without ring ribs. The radial unit force acts with excitation frequency range 10 Hz-4kHz. The observation point located at position (0.3 m, 0°, 1.2 m), in which acoustic responses of Model VI are calculated by coupled FEM/BEM. C3D8R elements in software ABAQUS are employed to generate linear hexahedron meshes of the cylindrical shell, the size of which is set to 4 mm. The external flow field radius is taken as 2 m. A hemispherical flow field is meshed by AC3D4 acoustic tetrahedral elements, the size of which is from 0.004 m to 0.0125 m. The results comparison of radiated noises at the observation point between the present method and coupled FEM/BEM is shown in Fig. 9.

The results from the present method are consistent with the results from coupled FEM/BEM at 10 Hz–2100 Hz. Although the sound pressure level is slightly different at the resonance peak value in the 2100~4 kHz range, the sound pressure values resulted from the present method is in accord with numerical results basically. There are many reasons for the difference. The process of equal divisions along the integral interval in Eq. (14) could cause the error of approximation. Both the substitution of the finite field for infinite fluid field and the setting of Tie connection at the interface also lead to the numerical error in software ABAQUS. The comparison provides the validity and reliability of the present method, which can be applied to sound radiation of immersed cylindrical shells with the variable thickness.

d) Comparison analysis: Model VII

The test model of a ring-stiffened cylindrical shell is constructed and prepared to prove the effectiveness of the present method. Model VII has the following material properties: Length $L = 0.8$ m, Radius $R = 0.3$ m. Shell thickness $t = 4$ mm. Sectional dimensions of the stiffener is 40 mm × 4 mm. The stiffeners spacing $\Delta l = 0.16$ m. The other physical parameters are the same as the Model IV. 15 mm thick caps are screwed at the ends of the cylinder. The shaker is fixed on the end cap in order to excite the point (0.4 m,0°,0.3 m) of Model VII. There are 3 hydrophones (BK-8104) is placed 1.0 m far from the cylindrical shell, which was set up in the anechoic tank to measure the sound pressure. Comparison of sound radiation curves between model test and the present method with the linear sweep frequency (100 Hz-2kHz) is given in Fig. 10. It can be observed that although the sound pressure is slightly different at the resonance peak value in the 500–2000 Hz band, the sound pressure result from PTMM basically is in accord with test result. When the internal medium of the experimental model is full of air, the coupling between structural mode and acoustic cavity mode has little effect on the vibro-acoustic response of the cylindrical shell. In general the present method provides enough verification and accuracy, which can be applied to vibro-acoustic behaviours of immersed stiffened cylindrical shells.

4. Conclusions

The vibro-acoustic model of the immersed stiffened cylindrical shell with various thickness is developed in this paper to predict the vibro-acoustic performance by combining PTMM and PWSM. Based on thin shell theory, a global matrix formulation as the governing equation is constructed with a set of field matrixes of stiffened cylindrical shell segments with various thickness. Then the dynamic behaviours can be directly solved by PTMM. The fluid load simulated by PWSM is employed to evaluate the radiated noise of the immersed cylindrical shell. Free vibration of three different cylindrical shells including cylindrical shell, immersed cylindrical shell and variable-thickness cylindrical shell are constructed and analyzed to illustrates the feasibility of the present method. Acoustic responses of four different cylindrical shells including cylindrical shell, immersed cylindrical shell, stiffened cylindrical shell and variable-thickness cylindrical shell are also constructed and analyzed to demonstrate its effectiveness. It is worth to point out that the proposed method is conveniently extended to analyze the vibro-acoustic behaviours of other elastic shells like conical shells, double-walled shells and combined shells with various thickness.

Acknowledgements

The authors would like to thank the anonymous reviewers for their valuable comments. This paper was financially supported by China Scholarship Council (201806955052), National Natural Science Foundation of China (51779201, 51609190) and Natural Science Foundation of Hubei Province (2018CFB607).

Appendix A

$$\boldsymbol{Tr}(i,\ i) = 1, i = 1, 2, 3 \cdots 8$$

$$\boldsymbol{Tr}(5,\ 1) = -\frac{R}{K}\left\{\left[\frac{EI_2}{R_b^3}n^2 + \frac{GJ}{R_b^3}n^2\right]h + eh\left[\frac{EI_2}{R_b^4}n^4 + \frac{GJ}{R_b^4}n^2 - \rho A\omega^2\right]\right\}$$

$$\boldsymbol{Tr}(5,\ 4) = -\frac{h}{K}\left\{\begin{array}{l}\left[\frac{EI_2}{R_b^3}R_b - \frac{EI_2}{R_b^3}en^2 - \frac{GJ}{R_b^3}en^2 + \frac{GJ}{R_b^3}R_b n^2 - \rho I_p\omega^2\right] \\ +e\left[-\frac{EI_2}{R_b^4}en^4 + \frac{EI_2}{R_b^4}Rn^2 - \frac{GJ}{R_b^4}en^2 + \frac{GJ}{R_b^4}Rn^2 - \rho A\omega^2 e\right]\end{array}\right\}$$

$$\boldsymbol{Tr}(6,\ 2) = -h\frac{R^2}{K}\left[\frac{EI_1}{R_b^4}\frac{R_b}{R}n^3 + \frac{EA}{R_b^2}\frac{R_b}{R}\right]$$

$$\boldsymbol{Tr}(6,\ 3) = -h\frac{R^2}{K}\left[\frac{EI_1}{R_b^4}\frac{R_b}{R}n^4 + \frac{EA}{R_b^2}\left(1+\frac{e}{R}n^2\right) - \rho A\omega^2\right]$$

$$\boldsymbol{Tr}(7,\ 2) = -h\frac{R^2}{K}\left[\frac{EI_1}{R_b^4}\frac{R_b}{R}n^2 + \frac{EA}{R_b^2}\frac{R_b}{R}n^2 - \rho A\omega^2\frac{R_b}{R}\right]$$

$$\boldsymbol{Tr}(7,\ 3) = -h\frac{R^2}{K}\left[\frac{EI_1}{R_b^4}\frac{R_b}{R}n^3 + \frac{EA}{R_b^2}n\frac{R-e}{R} - \rho A\omega^2 n\frac{e}{R}\right]$$

$$\boldsymbol{Tr}(8,\ 1) = -h\frac{R^2}{K}\left[\frac{EI_2}{R_b^4}n^4 + \frac{GJ}{R_b^4}n^2 - \rho A\omega^2\right]$$

$$\boldsymbol{Tr}(8,\ 4) = \frac{h}{R}\frac{R^2}{K}\left[-\frac{EI_2}{R_b^4}en^4 + \frac{EI_2}{R_b^4}R_1n^2 - \frac{GJ}{R_b^4}en^2 + \frac{GJ}{R_b^4}R_1n^2 - \rho A\omega^2 e\right]$$

where $R_b = R + e$ e is the offset of the rib. E, G are the Modulus of elasticity and shear of the rib. ρ is the density of the rib. A is the sectional area of the rib. I_1, I_2 and J are the moment of inertia in x-direction, y-direction and polar moment of inertia.

References

Caresta, M., Kessissoglou, N.J., 2009. Structural and acoustic responses of a fluid-loaded cylindrical hull with structural discontinuities. Appl. Acoust. 70 (7), 954–963.

El-Kaabazi, N., Kennedy, D., 2012. Calculation of natural frequencies and vibration modes of variable thickness cylindrical shells using the Wittrick–Williams algorithm. Comput. Struct. 104, 4–12.

Jin, G., Ma, X., Liu, Z., Xuan, L., 2017. Dynamic analysis of general rotationally symmetric built-up structures using a modified fourier spectral element approach. J. Vib. Acoust. 139 (2), 021012.

Laulagnet, B., Guyader, J., 1989. Modal analysis of a shell's acoustic radiation in light and heavy fluids. J. Sound Vib. 131 (3), 397–415.

Liu, C.-H., Chen, P.-T., 2009. Numerical analysis of immersed finite cylindrical shells using a coupled BEM/FEM and spatial spectrum approach. Appl. Acoust. 70 (2), 256–266.

Petyt, M., Lim, S., 1978. Finite element analysis of the noise inside a mechanically excited cylinder. Int. J. Numer. Methods Eng. 13 (1), 109–122.

Sandman, B., 1976. Fluid-loading influence coefficients for a finite cylindrical shell. J. Acoust. Soc. Am. 60 (6), 1256–1264.

Stepanishen, P.R., 1982. Modal coupling in the vibration of fluid-loaded cylindrical shells. J. Acoust. Soc. Am. 71 (4), 813–823.

Tang, D., Yao, X., Wu, G., Peng, Y., 2017. Free and forced vibration analysis of multi-stepped circular cylindrical shells with arbitrary boundary conditions by the method of reverberation-ray matrix. Thin-Walled Struct. 116, 154–168.

Tottenham, H., Shimizu, K., 1972. Analysis of the free vibration of cantilever cylindrical thin elastic shells by the matrix progression method. Int. J. Mech. Sci. 14 (5), 293–310.

Ventsel, E., Naumenko, V., Strelnikova, E., Yeseleva, E., 2010. Free vibrations of shells of revolution filled with a fluid. Eng. Anal. Bound. Elem. 34 (10), 856–862.

Wang, X., Wu, W., Yao, X., 2015. Structural and acoustic response of a finite stiffened conical shell. Acta Mech. Solida Sin. 28 (2), 200–209.

Wang, X., Guo, W., 2016a. Dynamic modeling and vibration characteristics analysis of submerged stiffened combined shells. Ocean Eng. 127, 226–235.

Wang, X.-z., Jiang, C.-b., Xu, R.-y., 2016b. Structural and acoustic response of a finite stiffened submarine hull. China Ocean Eng. 30 (6), 898–915.

Zhang, X., 2002. Frequency analysis of submerged cylindrical shells with the wave propagation approach. Int. J. Mech. Sci. 44 (7), 1259–1273.